Letter

Spin transport in a Berezinskii-Kosterlitz-Thouless magnet candidate $BaNi_2V_2O_8$

Kurea Nakagawa [1], Minoru Kanega [2], Tomoyuki Yokouchi [3], Masahiro Sato,[2] and Yuki Shiomi [1]

[1]Department of Basic Science, The University of Tokyo, Tokyo 153–8902, Japan
[2]Department of Physics, Chiba University, Chiba 263–8522, Japan
[3]RIKEN Center for Emergent Matter Science (CEMS), Wako 351-0198, Japan

(Received 25 December 2023; revised 22 July 2024; accepted 16 January 2025; published 29 January 2025)

In two-dimensional (2D) spin systems, the augmentation of spin fluctuations gives rise to quasi-long-range order; however, how they manifest in spin transport remains unclear. Here, we investigate the spin Seebeck effect (SSE) in a quasi-2D antiferromagnet, $BaNi_2V_2O_8$, which has been reported to exhibit the Berezinskii-Kosterlitz-Thouless (BKT) transition owing to its very weak interlayer interaction. We found that the SSE in $Pt/BaNi_2V_2O_8$ persists well above the Néel temperature, significantly different from the behavior of 3D-ordered magnets. Our numerical analysis for a 2D microscopic spin model confirms that the observed SSE is linked to the gapless magnon excitations and strong magnetic correlations characteristic of BKT magnets.

DOI: 10.1103/PhysRevMaterials.9.L011401

Introduction. Spin current generation [1] is a crucial technique finding its applications in spintronics and next-generation information processing. Not only does it have engineering significance, but it is also fundamentally important as an effective method for elucidating the spin excitation and transport of magnetic states. One of the most versatile methods for driving spin current is the spin Seebeck effect (SSE) [2–5]. The SSE refers to the generation of a spin current in a magnetic material in response to a temperature gradient across the junction between a magnetic material and a metal. Thanks to its simple bilayer structure and straightforward nature, the SSE serves as a valuable tool for investigating the spin dynamics in diverse magnetic insulators [3,6–21]. Recently, it has also been applied to exotic magnetic systems that lack long-range magnetic order but exhibit strong spin correlations, such as a 1D quantum spin liquid [22], a spin-nematic liquid [23], a spin-Peierls magnet [24], and a magnon-BEC magnet [25]. In such exotic magnetic systems, spin excitations are not described by the standard magnons in ordered magnets, and unique spin transport phenomena appear. The spin transport beyond the standard magnon picture has expanded material systems for spin current studies. The robust spin transport against external magnetic fields and the absence of stray magnetic fields may offer fundamental scientific insights as well as practical technological potential.

In the realm of exotic magnetic dynamics, two-dimensional (2D) spin systems, where magnetic interactions are dominant within a two-dimensional plane due to the very weak interlayer interactions, are particularly intriguing because of their enhanced spin fluctuations. In the case of a 2D Heisenberg magnet, long-range magnetic order is forbidden at finite temperatures [26,27]; instead, it exhibits a quasi-long-range order in a magnetic field, accompanied by the Berezinskii-Kosterlitz-Thouless (BKT) transition [28–32]. The BKT transition is a phase transition involving a change from bound vortex-antivortex pairs state (referred to as a BKT phase) at low temperatures to unpaired vortices and antivortices state at high temperatures within two-dimensional planes. It requires strong two-dimensionality, coexisting with enhanced spin fluctuations. This transition is known to display extremely subtle singularities that are considered undetectable by usual spin probes. While BKT transitions and their related topics in 2D or quasi-2D spin systems have long been explored mainly focusing on thermodynamic quantities, the effect of spin fluctuations in such systems on transport and nonequilibrium properties remains elusive. Moreover, a BKT transition has been reported in a monolayer van der Waals magnet due to its enhanced perpendicular magnetic anisotropy [33]. Understanding spin dynamics in BKT magnets can contribute to the emerging spintronic research field in van der Waals devices.

Although SSE in a layered ferromagnetic insulator with weak anisotropy in exchange coupling has been reported [34], highly 2D spin systems exhibiting BKT-like behavior have not yet been experimentally explored. Furthermore, since very recent theoretical works have revealed a novel contribution of the BKT spin texture to the spin current [35,36], the experimental study of spin current transport in BKT magnets is timely.

As a promising candidate for realizing 2D spin systems with BKT transitions, $BaNi_2V_2O_8$ stands out as a rare example in which a BKT-like transition has been experimentally confirmed. Its trigonal crystal structure houses spin-1 Ni^{2+} magnetic ions, forming honeycomb layers stacked parallel to the c axis [Fig. 1(a)]. As illustrated in Fig. 1(b), spins of Ni^{2+} ions lie within the honeycomb plane in the ground state, displaying a dominant antiferromagnetic exchange interaction between the nearest-neighbor Ni^{2+} ions. $BaNi_2V_2O_8$ is a quasi-2D Heisenberg antiferromagnet ($T_N = 47.75 \pm 0.25$ K) with weak XY anisotropy [37,38]. Magnetic susceptibility and specific heat do not show any sharp transitions associated with long-range magnetic ordering [37,38]. This pronounced 2D magnetic characteristic is mainly due to its outstandingly weak interlayer interaction ($|J_{out}| < 10^{-4} J_1$, where J_{out} and J_1 are interlayer and nearest-neighbor intralayer exchange interaction, respectively) [38]. The

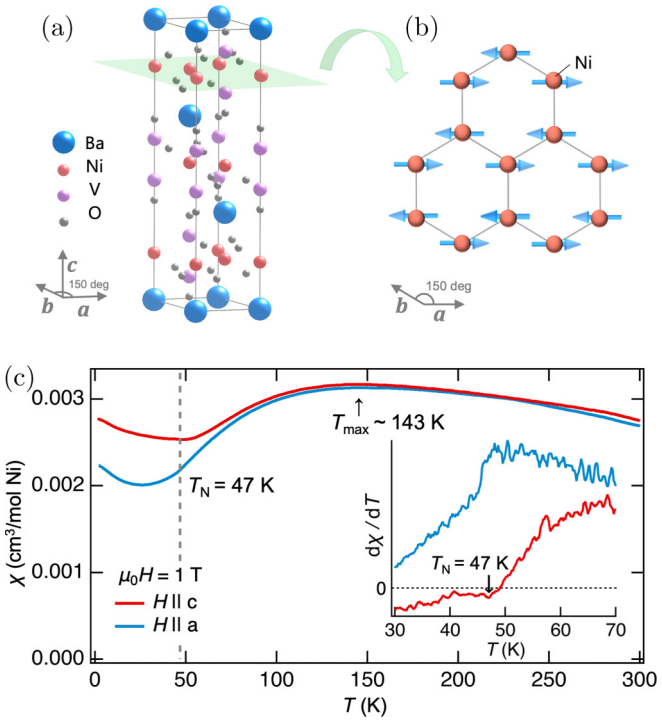

FIG. 1. (a) Crystal structure of $BaNi_2V_2O_8$. (b) Magnetic structure of a Ni^{2+} honeycomb plane. Each magnetic moment lies approximately in the honeycomb plane. (c) Temperature dependence of magnetic susceptibility χ at 1 T. The inset shows the temperature dependence of $\frac{d\chi}{dT}$ and the definition of T_N.

BKT-like transition has been experimentally confirmed by the critical scaling of the correlation length extracted from the linewidth of the electron spin resonance [39], spin-lattice relaxation rate of the nuclear magnetic resonance [40], and the inverse full-width half maximum of the neutron scattering measurements [41], reporting that the BKT-like transition temperature (T_{BKT}) lies between 40 and 45 K, just below T_N. It is known that layered magnets with weak interlayer interactions can undergo a magnetic transition above the BKT transition temperature [42,43]. In the presence of interlayer interactions, the BKT transition becomes a crossover [44], but strong 2D spin fluctuations associated with vortex excitations still persist over a broad temperature range.

In this study, we have investigated SSE in $BaNi_2V_2O_8$: a quasi-2D antiferromagnet with a BKT-like transition. The SSE of $Pt/BaNi_2V_2O_8-(100)$ significantly persists even above the Néel temperature, without any anomalies at the transition temperature, in contrast to the behavior of three-dimensional (3D) ordered magnets. Interestingly, these results are consistent with the calculation results for a weakly anisotropic 2D Heisenberg antiferromagnet with the BKT transition, which does not show long-range order. Therefore, the SSE in this system plausibly originates from strong magnetic correlations characteristic to the BKT spin systems over a very broad temperature range, despite $BaNi_2V_2O_8$ exhibiting magnetic order at low temperatures in a static sense.

Methods. Synthesis of single crystals of $BaNi_2V_2O_8$ and the SSE device fabrication are described in the Supplemental Material (SM) [45]. Magnetization was measured using a superconducting magnet Quantum Design MPMS3. The SSE devices used in the present study consist of a 5 nm thick Pt film sputtered on top of a $BaNi_2V_2O_8$ single crystal. The samples have a surface size of $0.9 \times 0.25-0.4\,mm^2$ with a thickness of 0.23 to 0.29 mm. In this study, the SSE was measured using a self-heating method [46] in a Quantum Design PPMS9. The Pt layer was utilized not only as a detection layer for spin currents but also as a heater to generate thermal gradients. An ac current $I_c \propto \sin \omega t$ was applied to the Pt film, generating a temperature gradient across $Pt/BaNi_2V_2O_8$ bilayer due to the Joule heating. Thermally induced spin current with 2 ω frequency produces inverse spin Hall effect signal in the Pt layer as a second harmonic voltage. By measuring the second-harmonic voltage $V_{2\omega}$ using a lock-in amplifier (NF LI5650) under magnetic fields applied perpendicular to both ac current and temperature gradient, we selectively detected the SSE signal. The typical parameters of the ac current were the amplitude of 4.5 to 6 mA and the frequency of 83 Hz (see also SM [45]). We normalized the detected voltage by the power of the applied current owing to its accuracy and reproducibility [47,48].

Results. We first examined the magnetic properties of $BaNi_2V_2O_8$. Magnetization shows a linear magnetic field dependence over the entire temperature range (see SM [45]). Temperature dependence of magnetic susceptibility χ, shown in Fig. 1(c), takes a characteristic behavior with a very broad peak around $T_{max} \sim 143$ K. At temperatures below the broad maximum, the susceptibility gradually decreases, and the anisotropy becomes more pronounced as temperature decreases. A small tail observed at very low temperatures is attributed to paramagnetic impurities, which have been frequently observed in this material [37,38] and other low-dimensional materials [49,50]. The Néel temperature is determined to be $T_N = 47$ K from the local minimum point of $\frac{d\chi_{H\|c}}{dT}$, following previous studies [38,41]. It is notable that the large T_{max}/T_N ratio highlights low-dimensional magnetism, and strong short-range correlations remain far above the transition temperature. The value of T_N, as well as the overall temperature dependence of magnetic susceptibility, are consistent with those of previous studies [37,38,41]. This indicates that the sample used in this study possesses a similar high degree of two-dimensionality as reported in earlier studies, although the BKT transition cannot generally be detected in magnetic susceptibility.

The SSE for $BaNi_2V_2O_8$ was then measured for two different configurations, as illustrated in Figs. 2(a) and 2(b): 5-nm-thick Pt films were sputtered on the (100)- or (001)-crystalline plane of $BaNi_2V_2O_8$, which corresponds to the configuration where the 2D honeycomb plane is perpendicular or parallel to the Pt plane, respectively. In Fig. 2(c), the magnetic field dependence of $V_{2\omega}$ at 20 K ($< T_N$) is shown. We first notice that the $V_{2\omega}$ of Pt/SiO_2 control sample is almost independent of the magnetic field. Here, SiO_2 means a thermally oxidized Si substrate that is diamagnetic, and thus Pt/SiO_2 is expected to exhibit a voltage solely from the normal Nernst effect of Pt [51]. From this result, we confirmed that the Nernst effect in Pt is too small to be detected in our devices. In contrast to Pt/SiO_2, both $Pt/BaNi_2V_2O_8$ devices show positive monotonic magnetic-field dependences, which can be attributed to the SSE signal. The positive sign

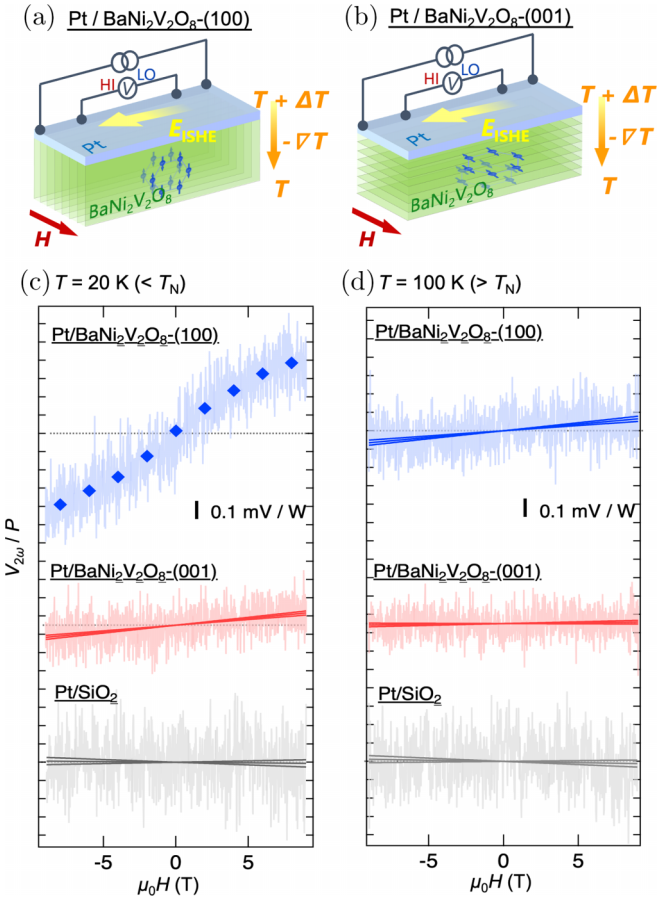

FIG. 2. (a),(b) Schematics of the SSE measurement setup for (a) $Pt/BaNi_2V_2O_8-(100)$ and (b) $Pt/BaNi_2V_2O_8-(001)$ shown with the 2D honeycomb planes. (c),(d) Magnetic-field dependence of $V_{2\omega}/P$ in $Pt/BaNi_2V_2O_8-(100)$, $Pt/BaNi_2V_2O_8-(001)$, and Pt/SiO_2 at (c) 20 K and (d) 100 K. Straight lines represent the linear fits; fitting errors were assessed with the confidence range of 99.73%. The diamond symbols in (c) show the representative points averaged over every 2 T.

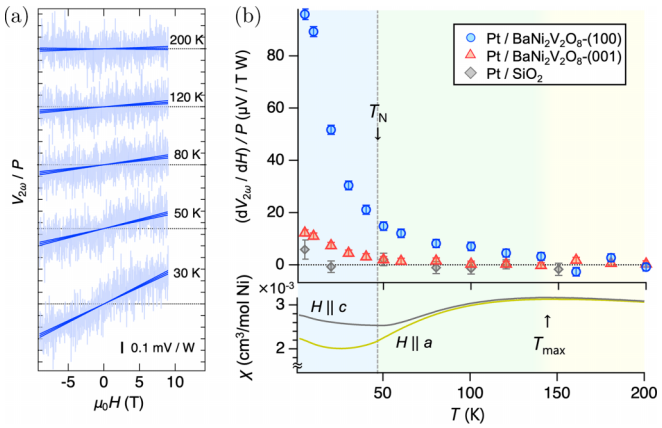

FIG. 3. (a) Magnetic-field dependence of $V_{2\omega}/P$ in $Pt/BaNi_2V_2O_8-(100)$ at various temperatures. (b) Temperature dependence of $(dV_{2\omega}/dH)/P$ in $Pt/BaNi_2V_2O_8-(100)$, $Pt/BaNi_2V_2O_8-(001)$, and Pt/SiO_2. The error bars indicate the confidence range of 99.73%. For comparison with the magnetic properties, the temperature dependence of the magnetic susceptibility at 1 T [already shown in Fig. 1(d)] is redisplayed in the bottom panel.

of the SSE signals is the same as that of Pt/YIG, a typical ferrimagnetic SSE material (see SM [45]). We further verified that W (10 nm)/$BaNi_2V_2O_8-(100)$ shows the opposite sign of voltage response at 10 K, consistent with the opposite sign of the spin Hall angle in W [45] (see also Ref. [52] therein). Notably, the signal of $Pt/BaNi_2V_2O_8-(100)$ is larger than that of $Pt/BaNi_2V_2O_8-(001)$. This fact is in line with the 2D magnetic character of $BaNi_2V_2O_8$: For the $Pt/BaNi_2V_2O_8-(100)$ configuration, the spin current generated within the 2D plane can directly flow into the Pt, while for the $Pt/BaNi_2V_2O_8-(001)$ configuration, the spin current hardly flows due to the very weak interplane interaction.

Next, we show in Fig. 2(d) the results of the same measurement conducted at 100 K, well above the Néel temperature. At this temperature, Pt/SiO_2 and $Pt/BaNi_2V_2O_8-(001)$ show almost no magnetic-field dependence within the confidence range. Nevertheless, $Pt/BaNi_2V_2O_8-(100)$ still shows a finite SSE signal with a linear positive dependence on the magnetic field.

We systematically measured the temperature dependence of the SSE for $Pt/BaNi_2V_2O_8-(100)$, as shown in Fig. 3(a). In Fig. 3(b), the slope of the linear fit to the magnetic-field dependence of $V_{2\omega}/P$ is plotted. Although the SSE for $Pt/BaNi_2V_2O_8-(100)$ deviates slightly from the linear magnetic-field dependence at very low temperatures, as shown in Figs. 2(c) and 3(a), we employed a linear approximation in $|\mu_0 H| \leqq 9$ T for all temperatures to ensure a consistent evaluation over the entire temperature range. In $Pt/BaNi_2V_2O_8-(100)$, large positive SSE signals are observed at low temperatures and continue to increase divergently down to a very low temperature of 5 K. The spin current should thermodynamically go down to zero at zero temperature, so the peak structure is expected to appear at temperatures lower than those reached in the experiment. As the temperature increases, the SSE monotonically decreases, and interestingly, it exhibits no significant changes at T_N, reminiscent of previous studies of magnetic susceptibility and specific heat in which no anomaly was detected at T_N [37,38]. Upon further increasing the temperature, the SSE signal disappears at approximately 150 K. A significant point is that this temperature is close to T_{max}, at which the magnetic susceptibility reaches its maximum. If T_{max} corresponds to the onset temperature of the 2D magnetic character ($J_1 \simeq 12.3$ meV $\simeq 143$ K), the SSE signals can be attributed to strong short-range correlations in $BaNi_2V_2O_8$. In contrast, the SSE signals in $Pt/BaNi_2V_2O_8-(001)$ and Pt/SiO_2 above T_N are negligibly small; the SSE signals above T_N are unique to $Pt/BaNi_2V_2O_8-(100)$. When comparing the SSE magnitudes for $Pt/BaNi_2V_2O_8$ at around T_N with those for Pt/YIG at 250 K obtained using a similar self-heating method, both are of the same order of magnitude [46].

The long-tailed temperature dependence of the SSE signals even above the transition temperature is considerably different from the SSE reported for typical 3D magnets. In most cases, the SSE due to short-range correlations above the transition

temperature of 3D magnets is much smaller than that in the ordered phase and sometimes too small to be observed. For example, for a 3D ferrimagnet YIG, the SSE signals gradually decrease toward the Curie temperature, and there is almost no signal detected above that temperature [53]. Also, for a 3D antiferromagnet Cr_2O_3, the SSE signals gradually decrease with increasing temperature, and even before reaching the transition temperature, their magnitude decreases by more than two orders compared to the low-temperature signal [16]. This is because the spin current in the 3D-ordered phase is carried by spin-wave excitations (magnons) and magnon SSE rapidly decreases toward the ordering temperature owing to the suppression of magnon excitations. Although a finite SSE signal above the Néel temperature was reported for a 3D antiferromagnet FeF_2 thin film [54], there is a clear kink structure at the Néel temperature, representing a change in the origin of the SSE between below and above the ordering temperature. The temperature dependence of the SSE in these 3D magnets completely differs from what is observed here for $BaNi_2V_2O_8$.

For 2D spin systems, the SSE was studied for layered ferromagnetic insulators $CrSiTe_3$ and $CrGeTe_3$, and the thermal spin current flowing perpendicular to the 2D layers was measured [34]. The SSE signals were still observed above the Curie temperature and attributed to short-range ferromagnetic correlations reinforced by the Zeeman interaction. However, we point out that the anisotropy in the exchange coupling strength (~ 5 [55]) for these layered magnets is much weaker than that of the present system ($> 10^4$ [38]) and the magnetic transition is rather 3D in $CrGeTe_3$ [56]. Moreover, the SSE signals due to the short-range in-plane ferromagnetic correlations for these materials were suppressed by the out-of-plane correlations rapidly diminishing above the Curie temperature, which is in stark contrast to the present case where the SSE disappears almost at the onset temperature of 2D magnetism.

In addition to the long tail, we again note a low-temperature feature of $BaNi_2V_2O_8$. The SSE signal in 3D-ordered magnets usually exhibits a peak as a function of temperature because the magnon gap and the magnon-magnon interaction suppress the signal as temperature decreases and increases, respectively [57]. The continuous growth of the SSE even until 5 K is unique to $BaNi_2V_2O_8$ and consistent with the gapless nature of spin-wave excitations, as discussed below.

Discussion. To understand the observed SSE more deeply, we performed numerical calculations (see also SM [45]) based on the formalism of the tunnel spin current [5,18,19,22–24,58,59]. The terminology "tunnel" means that we consider a spin current injected from $BaNi_2V_2O_8$ to the attached metal Pt through a "quantum tunneling effect," owing to the effect of a weak but finite exchange interaction between localized spins of the magnet and conduction-electron spins of Pt. As the microscopic model for $BaNi_2V_2O_8$ [41], we adopted a 2D Heisenberg antiferromagnet with a small XY anisotropy on a honeycomb lattice. The existence of a field H or anisotropy D reduces the symmetry from SU(2) to U(1) type, and such 2D U(1)-symmetric models exhibit a BKT transition like the 2D XY model, regardless of ferro- or antiferromagnetic nature [31,32,45]. We computed the spin dynamics by solving the stochastic Landau-Lifshitz-Gilbert (LLG) equation [1] at finite temperatures to adequately incorporate significant

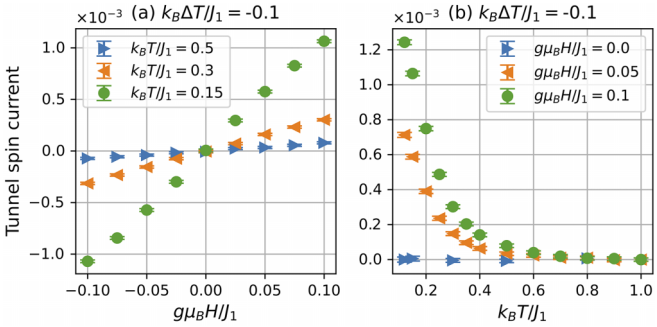

FIG. 4. (a) Magnetic-field and (b) temperature dependences of numerically calculated tunnel spin currents in the bilayer model of a 2D antiferromagnet (10×10 size) and a metal. Results of larger size systems also exhibit the same H and T dependences as the above panels (a) and (b) (see SM [45]). The temperature difference ΔT is defined as $\Delta T = T_{\rm metal} - T_{\rm magnet}$, where $T_{\rm metal}$ and $T_{\rm magnet}$ are, respectively, the temperatures of the metal and the antiferromagnet. Here, $g\mu_{\rm B}H = \frac{e\hbar}{m}\mu_0 H$. If we set $J_1 \simeq 12.3$ meV $\simeq 143$ K following Ref. [41], $k_{\rm B}T/J_1 = 0.15$, 0.3, and 0.5, respectively, correspond to $k_{\rm B}T \simeq 21$, 43, and 72 K. In addition, a magnetic field regime $|g\mu_{\rm B}H|/J_1 < 0.1$ corresponds to $|H| < 10.5$ T. The BKT transition point has been evaluated as $k_{\rm B}T_{\rm BKT} \sim 0.3\ J_1$ at $g\mu_{\rm B}H/J_1 \to 0$ [41]. From previous studies of Refs. [31,32], $k_{\rm B}T_{\rm BKT}$ is expected to be around $0.2\ J_1 < k_{\rm B}T_{\rm BKT} < 0.4\ J_1$ in a weak-field regime $|g\mu_{\rm B}H|/J_1 < 0.1$. The error bars indicate the confidence range of 99.73%.

thermal fluctuations in BKT magnets. The tunnel spin current in the metal partially changes into an electric current via the inverse spin Hall effect and the resulting SSE voltage is proportional to the tunnel spin current. The detail of the tunnel spin current analysis is in SM [45] (see also Refs. [60–64] therein).

Figure 4(a) shows the numerical result of the magnetic-field dependence of the tunnel spin current. The spin current monotonically increases with increasing field, and its sign is verified to be the same as that of the ferromagnet (see SM [45]). At $H = 0$, both spin-up and spin-down magnon densities are exactly the same and therefore the tunnel spin currents carried by up and down magnons cancel each other out. On the other hand, when a finite magnetization occurs by a positive field $H > 0$, down-spin magnons are stabilized (i.e., their lifetime increases) and their density also increases. Thus, the cancellation is broken and the tunnel spin current grows together with H. We also find from Fig. 4(b) that the spin current shows a divergent behavior in a very low-temperature regime, and monotonically decreases with the increasing temperature. It persists even in $T > T_{\rm BKT}$, with no characteristic change around $T = T_{\rm BKT}$. This temperature dependence can be interpreted as follows: In the BKT phase, there are always gapless magnons (spin waves) [27], which are the main carriers of the tunnel spin current. The gapless magnon should be distinct from the usual magnon in ordered magnets. When the temperature grows up, the vortex-pairs increase and disturb the spin-wave propagation, resulting in a monotonic decrease in the tunnel spin current with the increasing temperature. Even if the temperature becomes somewhat larger than $T_{\rm BKT}$, the spin correlation length is still long enough for the magnon

modes to survive at least for a short time and a short distance, giving rise to the finite tunnel spin current in $T > T_{BKT}$. These magnetic field and temperature dependence of the calculated tunnel spin currents are quite consistent with the observed SSE signals at a semi-quantitative level, and considerably different from the case of 3D-ordered magnets. This indicates that the spin current of the SSE in $BaNi_2V_2O_8$ is well described by the 2D antiferromagnetic model with a BKT transition in a broad temperature and magnetic-field regime.

Conclusion. We showed that the SSE in a BKT magnet candidate $BaNi_2V_2O_8$ is remarkably different from those in 3D magnets. In $Pt/BaNi_2V_2O_8-(100)$, the SSE signals are driven by the spin current flowing within the 2D honeycomb plane of $BaNi_2V_2O_8$, and notably persist well above the Néel temperature, without appreciable change at T_N and T_{BKT}. Reflecting its strong 2D characteristics, the SSE in $BaNi_2V_2O_8$ extends to a temperature almost three times higher than the Néel temperature, surpassing the temperature range reported in other 2D magnets with less anisotropy. Our numerical calculations indicate that the SSE observed over the entire temperature range is consistent with that expected in a 2D Heisenberg model exhibiting a BKT transition under a magnetic field. Hence, the SSE in the present system plausibly results from strong spin fluctuations, which are characteristic of 2D spin systems. Although $BaNi_2V_2O_8$ exhibits magnetic order at low temperatures in a static sense, our findings suggest that spin current transport in $BaNi_2V_2O_8$ captures the spin dynamics of the model calculation in a BKT system over a very broad temperature range across the Néel temperature. In addition, the detected SSE signals were comparable to those in the extensively studied ferrite YIG, even at and above T_N, highlighting the significance in the potential application of such 2D spin systems to spintronics devices.

The SSE measurements therefore provide a valuable tool for probing unique spin transport in BKT systems. More sophisticated measurements could offer deeper insights into the relationship between the observed SSE and BKT physics. For instance, spatially resolved SSE measurements might uncover the role of vortices in SSE, as the BKT transition is closely associated with vortex and antivortex excitations, whose size is typically nano- or micrometer scale. Moreover, time-resolved SSE measurements using optical probes may also be useful, although the temperature dependence is sometimes different from that observed in electrical measurements [65]. For example, they could reveal the scaling behavior of the correlation length during spin-current transport, considering recent advancements in ultrafast optical techniques to explore the BKT transition [66,67].

Acknowledgments. We thank Dr. Takashi Kikkawa and Prof. Hiroto Adachi for the fruitful discussions. This work was carried out by joint research of the Cryogenic Research Center, the University of Tokyo. This work was supported by the Japan Science and Technology Agency (JST) FOREST Program, Grant No. JPMJFR203H and by the Japan Society for the Promotion of Science (JSPS) KAKENHI, Grants No. JP22H05449, No. JP22H04464, No. JP23H01832, No. JP23H04576, No. JP23H01392, No. JP21H01794, No. JP23H04582, No. JP20H01830, No. JP20H01849, No. JP19H05825, No. JP19H05600, No. JP22H05131, No. JP23H04576, No. JP24K21726, No. JP24H01177, and No. JP24K00566. K.N. is supported by Research Fellowships of the Japan Society for the Promotion of Science for Young Scientists, Grant No. JP22KJ1068, and by Iketani Science and Technology Foundation, Grant No. 0361164-A. M.K. is supported by JST, the establishment of university fellowships toward the creation of science technology innovation, Grant No. JPMJFS2107. M.S. is supported by JST, CREST Grant No. JPMJCR24R5, Japan.

[1] *Spin Current*, edited by S. Maekawa, S. O. Valenzuela, E. Saitoh, and T. Kimura, (Oxford University Press, Oxford, 2017).

[2] K. Uchida, S. Takahashi, K. Harii, J. Ieda, W. Koshibae, K. Ando, S. Maekawa, and E. Saitoh, Observation of the spin Seebeck effect, Nature (London) **455**, 778 (2008).

[3] K. Uchida, H. Adachi, T. Ota, H. Nakayama, S. Maekawa, and E. Saitoh, Observation of longitudinal spin-Seebeck effect in magnetic insulators, Appl. Phys. Lett. **97**, 172505 (2010).

[4] T. Kikkawa and E. Saitoh, Spin Seebeck effect: Sensitive probe for elementary excitation, spin correlation, transport, magnetic order, and domains in solids, Annu. Rev. Condens. Matter Phys. **14**, 129 (2023).

[5] H. Adachi, J. Ohe, S. Takahashi, and S. Maekawa, Linear-response theory of spin Seebeck effect in ferromagnetic insulators, Phys. Rev. B **83**, 094410 (2011).

[6] A. Slachter, F. L. Bakker, J.-P. Adam, and B. J. van Wees, Thermally driven spin injection from a ferromagnet into a nonmagnetic metal, Nat. Phys. **6**, 879 (2010).

[7] K. Uchida, T. Nonaka, T. Ota, and E. Saitoh, Longitudinal spin-Seebeck effect in sintered polycrystalline (Mn, Zn)Fe_2O_4, Appl. Phys. Lett. **97**, 262504 (2010).

[8] K. Uchida, T. Nonaka, T. Kikkawa, Y. Kajiwara, and E. Saitoh, Longitudinal spin Seebeck effect in various garnet ferrites, Phys. Rev. B **87**, 104412 (2013).

[9] D. Meier, T. Kuschel, L. Shen, A. Gupta, T. Kikkawa, K. Uchida, E. Saitoh, J.-M. Schmalhorst, and G. Reiss, Thermally driven spin and charge currents in thin $NiFe_2O_4$/Pt films, Phys. Rev. B **87**, 054421 (2013).

[10] R. Ramos, T. Kikkawa, K. Uchida, H. Adachi, I. Lucas, M. H. Aguirre, P. Algarabel, L. Morellón, S. Maekawa, E. Saitoh, and M. R. Ibarra, Observation of the spin Seebeck effect in epitaxial Fe3O4 thin films, Appl. Phys. Lett. **102**, 072413 (2013).

[11] Y. Ohnuma, H. Adachi, E. Saitoh, and S. Maekawa, Spin Seebeck effect in antiferromagnets and compensated ferrimagnets, Phys. Rev. B **87**, 014423 (2013).

[12] S. M. Wu, J. E. Pearson, and A. Bhattacharya, Paramagnetic spin Seebeck effect, Phys. Rev. Lett. **114**, 186602 (2015).

[13] K. Oyanagi, S. Takahashi, T. Kikkawa, and E. Saitoh, Mechanism of paramagnetic spin Seebeck effect, Phys. Rev. B **107**, 014423 (2023).

[14] S. Seki, T. Ideue, M. Kubota, Y. Kozuka, R. Takagi, M. Nakamura, Y. Kaneko, M. Kawasaki, and Y. Tokura, Thermal

generation of spin current in an antiferromagnet, Phys. Rev. Lett. **115**, 266601 (2015).

[15] S. M. Wu, W. Zhang, A. KC, P. Borisov, J. E. Pearson, J. S. Jiang, D. Lederman, A. Hoffmann, and A. Bhattacharya, Antiferromagnetic spin Seebeck effect, Phys. Rev. Lett. **116**, 097204 (2016).

[16] J. Li, C. B. Wilson, R. Cheng, M. Lohmann, M. Kavand, W. Yuan, M. Aldosary, N. Agladze, P. Wei, M. S. Sherwin *et al.*, Spin current from sub-terahertz-generated antiferromagnetic magnons, Nature (London) **578**, 70 (2020).

[17] D. Reitz, J. Li, W. Yuan, J. Shi, and Y. Tserkovnyak, Spin Seebeck effect near the antiferromagnetic spin-flop transition, Phys. Rev. B **102**, 020408 (2020).

[18] Y. Yamamoto, M. Ichioka, and H. Adachi, Antiferromagnetic spin Seebeck effect across the spin-flop transition: A stochastic Ginzburg-Landau simulation, Phys. Rev. B **105**, 104417 (2022).

[19] K. Masuda and M. Sato, Microscopic theory of spin Seebeck effect in antiferromagnets, J. Phys. Soc. Jpn. **93**, 034702 (2024).

[20] J. Xu, J. He, J.-S. Zhou, D. Qu, S.-Y. Huang, and C. L. Chien, Observation of vector spin Seebeck effect in a noncollinear antiferromagnet, Phys. Rev. Lett. **129**, 117202 (2022).

[21] A. Mook, R. R. Neumann, J. Henk, and I. Mertig, Spin Seebeck and spin Nernst effects of magnons in noncollinear antiferromagnetic insulators, Phys. Rev. B **100**, 100401 (2019).

[22] D. Hirobe, M. Sato, T. Kawamata, Y. Shiomi, K. Uchida, R. Iguchi, Y. Koike, S. Maekawa, and E. Saitoh, One-dimensional spinon spin currents, Nat. Phys. **13**, 30 (2017).

[23] D. Hirobe, M. Sato, M. Hagihala, Y. Shiomi, T. Masuda, and E. Saitoh, Magnon pairs and spin-nematic correlation in the spin Seebeck effect, Phys. Rev. Lett. **123**, 117202 (2019).

[24] Y. Chen, M. Sato, Y. Tang, Y. Shiomi, K. Oyanagi, T. Masuda, Y. Nambu, M. Fujita, and E. Saitoh, Triplon current generation in solids, Nat. Commun. **12**, 5199 (2021).

[25] W. Xing, R. Cai, K. Moriyama, K. Nara, Y. Yao, W. Qiao, K. Yoshimura, and W. Han, Spin Seebeck effect in quantum magnet $Pb_2V_3O_9$, Appl. Phys. Lett. **120**, 042402 (2022).

[26] N. D. Mermin and H. Wagner, Absence of ferromagnetism or antiferromagnetism in one- or two-dimensional isotropic Heisenberg models, Phys. Rev. Lett. **17**, 1133 (1966).

[27] H. Nishimori and G. Ortiz, *Elements of Phase Transitions and Critical Phenomena* (Oxford University Press, Oxford, United Kingdom, 2011).

[28] V. L. Berezinskii, Destruction of long-range order in one-dimensional and two-dimensional systems having a continuous symmetry group I. Classical system, Sov. Phys. JETP **32**, 493 (1971).

[29] J. M. Kosterlitz and D. J. Thouless, Long range order and metastability in two dimensional solids and superfluids. (Application of dislocation theory), J. Phys. C: Solid State Phys. **5**, L124 (1972).

[30] J. M. Kosterlitz, The critical properties of the two-dimensional XY model, J. Phys. C: Solid State Phys. **7**, 1046 (1974).

[31] D. P. Landau and K. Binder, Phase diagrams and critical behavior of a two-dimensional anisotropic Heisenberg antiferromagnet, Phys. Rev. B **24**, 1391 (1981).

[32] A. Cuccoli, T. Roscilde, R. Vaia, and P. Verrucchi, Field-induced XY behavior in the $S = 1/2$ antiferromagnet on the square lattice, Phys. Rev. B **68**, 060402 (2003).

[33] A. Bedoya-Pinto, J.-R. Ji, A. K. Pandeya, P. Gargiani, M. Valvidares, P. Sessi, J. M. Taylor, F. Radu, K. Chang, and S. S. P. Parkin, Intrinsic 2D-XY ferromagnetism in a van der Waals monolayer, Science **374**, 616 (2021).

[34] N. Ito, T. Kikkawa, J. Barker, D. Hirobe, Y. Shiomi, and E. Saitoh, Spin Seebeck effect in the layered ferromagnetic insulators $CrSiTe_3$ and $CrGeTe_3$, Phys. Rev. B **100**, 060402 (2019).

[35] R. J. C. Lopes, A. R. Moura, and W. A. Moura-Melo, Berezinskii-Kosterlitz-Thouless transition effects on spin current: The normal-metal-insulating-ferromagnet junction case, Phys. Rev. B **102**, 184422 (2020).

[36] S. K. Kim and S. B. Chung, Transport signature of the magnetic Berezinskii-Kosterlitz-Thouless transition, SciPost Phys. **10**, 068 (2021).

[37] N. Rogado, Q. Huang, J. W. Lynn, A. P. Ramirez, D. Huse, and R. J. Cava, $BaNi_2V_2O_8$: A two-dimensional honeycomb antiferromagnet, Phys. Rev. B **65**, 144443 (2002).

[38] E. S. Klyushina, B. Lake, A. T. M. N. Islam, J. T. Park, A. Schneidewind, T. Guidi, E. A. Goremychkin, B. Klemke, and M. Månsson, Investigation of the spin-1 honeycomb antiferromagnet $BaNi_2V_2O_8$ with easy-plane anisotropy, Phys. Rev. B **96**, 214428 (2017).

[39] M. Heinrich, H.-A. Krug Von Nidda, A. Loidl, N. Rogado, and R. J. Cava, Potential signature of a Kosterlitz-Thouless transition in $BaNi_2V_2O_8$, Phys. Rev. Lett. **91**, 137601 (2003).

[40] D. Waibel, G. Fischer, Th. Wolf, H. V. Löhneysen, and B. Pilawa, Determining the Berezinskii-Kosterlitz-Thouless coherence length in $BaNi_2V_2O_8$ by ^{51}V NMR, Phys. Rev. B **91**, 214412 (2015).

[41] E. S. Klyushina, J. Reuther, L. Weber, A. T. M. N. Islam, J. S. Lord, B. Klemke, M. Månsson, S. Wessel, and B. Lake, Signatures for Berezinskii-Kosterlitz-Thouless critical behavior in the planar antiferromagnet $BaNi_2V_2O_8$, Phys. Rev. B **104**, 064402 (2021).

[42] S. Hikami and T. Tsuneto, Phase transition of quasi-two dimensional planar system, Prog. Theor. Phys. **63**, 387 (1980).

[43] S. T. Bramwell and P. C. W. Holdsworth, Magnetization and universal sub-critical behaviour in two-dimensional XY magnets, **5**, L53 (1993).

[44] V. Y. Irkhin and A. A. Katanin, Kosterlitz-Thouless and magnetic transition temperatures in layered magnets with a weak easy-plane anisotropy, Phys. Rev. B **60**, 2990 (1999).

[45] See Supplemental Material at http://link.aps.org/supplemental/10.1103/PhysRevMaterials.9.L011401 for the experimental and numerical confirmation of the SSE, and theoretical details of the tunnel spin current, which also includes Refs. [1,3,5,8,18,19,22–24,26,27,31,32,37,41,57,59–64].

[46] M. Schreier, N. Roschewsky, E. Dobler, S. Meyer, H. Huebl, R. Gross, and S. T. B. Goennenwein, Current heating induced spin Seebeck effect, Appl. Phys. Lett. **103**, 242404 (2013).

[47] A. Sola, P. Bougiatioti, M. Kuepferling, D. Meier, G. Reiss, M. Pasquale, T. Kuschel, and V. Basso, Longitudinal spin Seebeck coefficient: Heat flux vs. temperature difference method, Sci. Rep. **7**, 46752 (2017).

[48] A. Prakash, B. Flebus, J. Brangham, F. Yang, Y. Tserkovnyak, and J. P. Heremans, Evidence for the role of the magnon energy relaxation length in the spin Seebeck effect, Phys. Rev. B **97**, 020408 (2018).

[49] D. Bono, L. Limot, P. Mendels, G. Collin, and N. Blanchard, Correlations, spin dynamics, defects: The highly frustrated kagome bilayer, Low Temp. Phys. **31**, 704 (2005).

[50] H. Lu, T. Yamamoto, W. Yoshimune, N. Hayashi, Y. Kobayashi, Y. Ajiro, and H. Kageyama, A nearly ideal one-dimensional $S = 5/2$ antiferromagnet $FeF_3(4, 4'-bpy)$ $(4, 4'-bpy = 4, 4'-bipyridyl)$ with strong intrachain interactions, J. Am. Chem. Soc. **137**, 9804 (2015).

[51] A. Chanda, C. Holzmann, N. Schulz, J. Seyd, M. Albrecht, M. Phan, and H. Srikanth, Scaling of the thermally induced sign inversion of longitudinal spin Seebeck effect in a compensated ferrimagnet: Role of magnetic anisotropy, Adv. Funct. Mater. **32**, 2109170 (2022).

[52] A. Hoffmann, Spin Hall effects in metals, IEEE Trans. Magn. **49**, 5172 (2013).

[53] K. Uchida, T. Kikkawa, A. Miura, J. Shiomi, and E. Saitoh, Quantitative temperature dependence of longitudinal spin Seebeck effect at high temperatures, Phys. Rev. X **4**, 041023 (2014).

[54] J. Li, Z. Shi, V. H. Ortiz, M. Aldosary, C. Chen, V. Aji, P. Wei, and J. Shi, Spin Seebeck effect from antiferromagnetic magnons and critical spin fluctuations in epitaxial FeF_2 films, Phys. Rev. Lett. **122**, 217204 (2019).

[55] T. J. Williams, A. A. Aczel, M. D. Lumsden, S. E. Nagler, M. B. Stone, J.-Q. Yan, and D. Mandrus, Magnetic correlations in the quasi-two-dimensional semiconducting ferromagnet $CrSiTe_3$, Phys. Rev. B **92**, 144404 (2015).

[56] G. T. Lin, H. L. Zhuang, X. Luo, B. J. Liu, F. C. Chen, J. Yan, Y. Sun, J. Zhou, W. J. Lu, P. Tong *et al.*, Tricritical behavior of the two-dimensional intrinsically ferromagnetic semiconductor $CrGeTe_3$, Phys. Rev. B **95**, 245212 (2017).

[57] T. Kikkawa, K. Uchida, S. Daimon, Z. Qiu, Y. Shiomi, and E. Saitoh, Critical suppression of spin Seebeck effect by magnetic fields, Phys. Rev. B **92**, 064413 (2015).

[58] Y. Kato, J. Nasu, M. Sato, T. Okubo, T. Misawa, and Y. Motome, Spin seebeck effect as a probe for majorana fermions in Kitaev spin liquids, arXiv:2401.13175.

[59] A.-P. Jauho, N. S. Wingreen, and Y. Meir, Time-dependent transport in interacting and noninteracting resonant-tunneling systems, Phys. Rev. B **50**, 5528 (1994).

[60] M. E. Fisher, M. N. Barber, and D. Jasnow, Helicity modulus, superfluidity, and scaling in isotropic systems, Phys. Rev. A **8**, 1111 (1973).

[61] Y. Tomita and Y. Okabe, Finite-size scaling of correlation ratio and generalized scheme for the probability-changing cluster algorithm, Phys. Rev. B **66**, 180401 (2002).

[62] P. Minnhagen and B. J. Kim, Direct evidence of the discontinuous character of the Kosterlitz-Thouless jump, Phys. Rev. B **67**, 172509 (2003).

[63] Y. Kumano, K. Hukushima, Y. Tomita, and M. Oshikawa, Response to a twist in systems with Z_p symmetry: The two-dimensional p-state clock model, Phys. Rev. B **88**, 104427 (2013).

[64] M. Sato, N. Watanabe, and N. Furukawa, Quasi long range order of defects in frustrated antiferromagnetic Ising models on spatially anisotropic triangular lattices, J. Phys. Soc. Jpn. **82**, 073002 (2013).

[65] F. N. Kholid, D. Hamara, M. Terschanski, F. Mertens, D. Bossini, M. Cinchetti, L. McKenzie-Sell, J. Patchett, D. Petit, R. Cowburn *et al.*, Temperature dependence of the picosecond spin Seebeck effect, Appl. Phys. Lett. **119**, 032401 (2021).

[66] U. F. P. Seifert, M. Ye, and L. Balents, Ultrafast optical excitation of magnetic dynamics in van der Waals magnets: Coherent magnons and BKT dynamics in $NiPS_3$, Phys. Rev. B **105**, 155138 (2022).

[67] L. Hu, H. -X. Wang, Y. Chen, K. Xu, M. -R. Li, H. Liu, P. Gu, Y. Wang, M. Zhang, H. Yao *et al.*, Observation of a magnetic phase transition in monolayer $NiPS_3$, Phys. Rev. B **107**, L220407 (2023).